

# Towards a Kernel based Physical Interpretation of Model Uncertainty

**Rishabh Singh**

**Jose C. Principe**

Computational NeuroEngineering Laboratory, Department of Electrical and Computer Engineering, University of Florida, Gainesville, FL 32611, USA

**Keywords:** Model uncertainty, RKHS, point-prediction, neural networks, quantum physics, moment decomposition

## **Abstract**

This paper introduces a new information theoretic framework that provides a sensitive multi-modal quantification of data uncertainty by leveraging a quantum physical description of its metric space. We specifically work with the kernel mean embedding metric which yields an intuitive physical interpretation of the signal as a *potential field*, resulting in its new energy based formulation. This enables one to extract multi-scale uncertainty features of data in the form of *information eigenmodes* by utilizing mo-

ment decomposition concepts of quantum physics. In essence, this approach decomposes local realizations of the signal's PDF in terms of quantum uncertainty moments. We specifically present the application of this framework as a non-parametric and non-intrusive surrogate tool for predictive uncertainty quantification of point-prediction neural network models, overcoming various limitations of conventional Bayesian and ensemble based UQ methods. Experimental comparisons with some established uncertainty quantification methods illustrate performance advantages exhibited by our framework.

## **1 Introduction**

### **1.1 Information Theory: Physics based Perspective**

The foundation of information theory lies in its ability to quantify uncertainty in random variables. This is primarily achieved by entropy, a metric having its origins in thermodynamics where it is used to describe micro-states of a system (Boltzmann, 1877). Shannon (Shannon & Weaver, 1949) first formulated entropy in the context of information theory which was later generalized by Renyi (Rényi et al., 1961) among many others. It has, since then, become an indispensable tool in density estimation and other statistical evaluations that attempt to characterize the intrinsic generating functions of data (Kullback & Leibler, 1951; Theil & Meisner, 1980; Hahn & Shapiro, 1967). However, since even before the introduction of Shannon's work, Fisher information (Fisher, 1922) has been well regarded as the cornerstone concept in measuring the gain of information from data and in quantifying the *order* of a system (Frieden & Hawkins, 2010),

instead of disorder as is done by entropy. This presents a strong link between the role of information in data analysis and physical laws (Frieden, 2004). Indeed, attempts to formulate quantum physical models of stock markets in the field of econophysics, for instance, have been quite prevalent in recent years (Meng et al., 2016; Ahn et al., 2018).

## **1.2 Motivation and Contributions**

### **Data Uncertainty Viewpoint**

In most real world scenarios, observed signals are generated by systems controlled by a multitude of source processes and noise resulting in very complicated data dynamics comprising of high uncertainty and stochasticity. Current machine learning models and information theoretic divergence measures fail to effectively characterize uncertainties associated with such data. Quantum based formulations in physics, on the other hand, have been well known for providing high resolution multi-scale characterizations of system dynamics. This is achieved through a stochastic description of the system in terms of energy modes in a Hilbert space of functions. The key qualities of such formulations is their non-parametric nature and a complete consideration for all internal associations of the system, leading to a description of the system at all points in space. We hypothesize that extending information theoretic measures in terms of such physics based formulations could yield similar advantages in the characterization of data and models, thereby providing us with a more enhanced view of information dynamics. This inspires us to develop data characterization tools that gather source information intrinsically from data while making minimal assumptions on their governing distributions, other than the fact that their generating processes follow laws of physics. Our

conjecture is that frameworks that work with the intrinsic stochasticities associated with local *data-induced* metric spaces would be significantly more sensitive towards signal characterization. Perhaps the best contender for this metric space is the Gaussian reproducing kernel Hilbert space (RKHS) which has been well established to provide universal characterization of data (Parzen, 1970; Rasmussen, 2003; Bergman, 1970; Vapnik, 2013). Moreover, projecting data into an RKHS transforms them into Gaussian functions centered at the data coordinates that obey the properties of a potential field (Principe, 2010). Hence the RKHS makes it possible to obtain quantum physical formulations of data properties with simplicity because of the uses of the Hilbert space.

Therefore, towards the goal of effectively quantifying data uncertainty, we introduce an RKHS based information theoretic framework that utilizes quantum physical interpretation of the data space to extract its various uncertainty moments. This methodology has solid foundations because it uses the kernel mean embedding (KME) metric (Muandet et al., 2017) which embeds the data into a kernel feature space and non-parametrically characterizes its PDF as an element in the RKHS. We show that the information potential field is an empirical estimate of the KME which eventually leads to a quantum physical energy-based description of the data structure in terms of a Schrödinger's equation. This allows us to extract the various modes of uncertainty related to the interaction of an upcoming data sample with the signal's history by implementing a moment decomposition procedure based on orthogonal polynomial projections, similar to that used in quantum physics to extract the eigenmodes of a particle with respect to its neighboring force field. We also refer to extracted data uncertainty modes as information eigenmodes since they are essentially *energy-based* information

features of data. Our uncertainty framework is depicted in fig. 1 and can be summarized in terms of the following key steps.

1. Definition of an RKHS based metric space using kernel mean embedding of data (information potential field).
2. Quantum physical energy-based formulation of the metric space in terms of the Schrödinger's equation.
3. Moment decomposition procedure involving orthogonal polynomial projections of the wave-function to extract uncertainty eigenstates from the quantum formulation.

Such a framework offers several key advantages. Firstly, owing to the use of a kernel based metric, our framework takes into account all intrinsic even order statistical moments (for the Gaussian kernel) and provides a universal characterization of data. Secondly, the quantum-physical formulation of the data space and its subsequent moment decomposition results in a high resolution (multi-scale) quantification of data uncertainties, which becomes increasingly sensitive at the tails of data distribution (where uncertainty is maximum). Lastly, the framework can be implemented in real time on

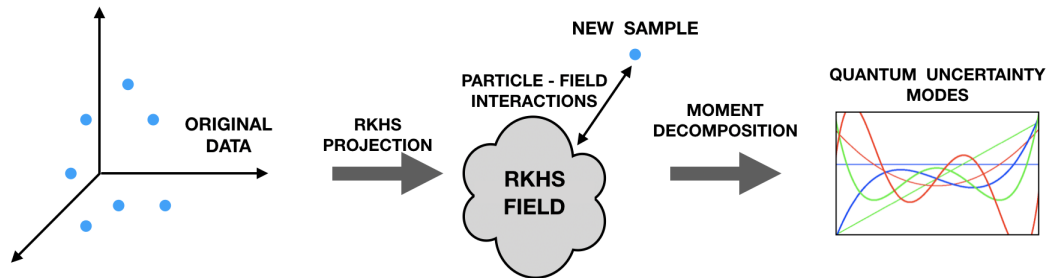


Figure 1: Basic depiction of the proposed framework

a sample-by-sample basis. The kernel metric and its associated quantum formulations adapt to new data thereby making it an appropriate feature extraction framework for streaming data.

### **Model Uncertainty Viewpoint**

In the world of machine learning, feedforward point-prediction neural network models have made remarkable progress over the past two decades in a large variety of applications (LeCun et al., 2015). However, despite their success, such models do not provide information related to their prediction uncertainties. This information is crucial in sensitive application arenas such as personalized medicine and autonomous driving, especially given how prone neural networks are towards overfitting. Moreover, there have also been alarming revelations regarding the high susceptibility of such models towards adversarial attacks (Su et al., 2019; Nguyen et al., 2015). All of this has led to a recent realization of the importance of uncertainty quantification of point-prediction models among the machine learning community thus making it an active area of research.

We are therefore motivated to explore the utility of our proposed framework for the predictive uncertainty quantification of point-prediction based learning models. The main idea here is to find the uncertain regions in the input-output mapping (instead of data space) learnt by the model. In this case, instead of working on data PDF, we propose a quantum based decomposition of the local realizations of distribution learnt by the model parameters based on the cross-entropy between the model output and its internal layers. This cross-entropy leads to the definition of the cross information potential. We hypothesize that such a decomposition of the model could yield useful

uncertainty information related to its predictions. Before delving into more details, we first review some established methods of uncertainty quantification (UQ).

Existing UQ methods can be broadly classified into *forward UQ* and *inverse UQ* methods from an implementation point of view (Smith, 2013; Sullivan, 2015). In uncertainty propagation (forward UQ), one attempts to directly characterize the model output uncertainty distribution from the implicit uncertainties present in the parameters. Inverse UQ, on the other hand, attempts to quantify uncertainty distributions over model parameters. In the context of machine learning, most of the focus has been on the latter category with a domination of Bayesian based inferencing methods which offer the most mathematically grounded approach to quantify model uncertainty by learning probability distributions of model weights (MacKay, 1992; Neal, 2012; Bishop, 1995). Early development of Bayesian based models revolved around Laplacian approximation (MacKay, 1992), Hamiltonian Monte Carlo (Neal, 2012), Markov-chain Monte Carlo (MCMC) based Bayesian neural networks (Bishop, 1995). Although such methods offer a principled approach of quantifying model uncertainty mainly by marginalizing over model parameters, they involve prohibitive computational costs and lack scalability towards large data and model architectures. Most of the recent work in this field has therefore been related to developing faster variational inference based approaches that offer more efficient ways of training Bayesian neural networks (BNNs) (Graves, 2011; Paisley et al., 2012; Hoffman et al., 2013). The high parameter dimensionality and the complexity of weight associations in modern neural networks still makes it very difficult for such variational inference approaches to adequately capture parameter dependencies (Pradier et al., 2018). Other methods involve surrogate modeling techniques that exploit

the input-output mapping learnt by the model (Nagel, 2017; Fang et al., 2005; Forrester et al., 2008). Here, computationally cheap approximations of models are used for easier extraction of the relevant information related to model uncertainty. Forward UQ methods include ensemble based methods where multiple instances of models with different initializations are trained on noisy data and the result is the aggregation of all model outputs (Tibshirani, 1996; Osband et al., 2016a; Pearce et al., 2018). The variations of the results provide the necessary uncertainty information. A notable related work is that of Lakshminarayan (Lakshminarayanan et al., 2017) where authors use ensemble neural networks to implement forward UQ. Recent work of Gal and Ghahramani (Gal & Ghahramani, 2016) has gained increased popularity due to its simplicity and effectiveness in quantifying predictive uncertainty. Here, authors propose Monte Carlo dropout where multiple instantiations of dropout are used during testing of models to obtain the uncertainty intervals associated with the model predictions.

We advocate an approach for predictive uncertainty quantification that is non-intrusive to the training process of a traditional point-prediction model and relies solely on extracting information from the internal dependencies of the *trained* model with respect to its output. In this regard, we hypothesize that the application of our framework as a forward UQ method could be advantageous. The idea is to create an alternate representation or an embedding of the learnt input-output mapping that makes it easier to quantify how uncertain (or probabilistically far) a prediction is with respect to it. Towards this end, we utilize our framework as a surrogate uncertainty quantifier of a trained neural network that constructs an RKHS embedding of the model’s discrete input-output mapping, realized at every test instance. This is done by projecting the model’s internal



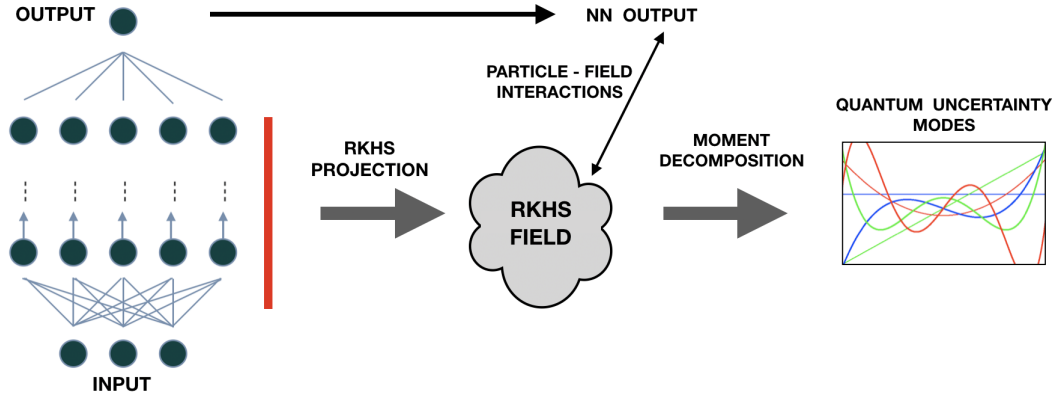


Figure 2: Implementation of proposed framework on a neural network.

activation outputs (from one or more layers) into the RKHS and empirically evaluating it with respect to the corresponding model prediction (implemented during each test cycle). Multi-scale uncertainty modes can then be extracted by the subsequent quantum physical formulations and moment decompositions implemented in the same manner as before. In simpler terms, we aim to utilize our framework to provide an alternate richer representation of the model-output dynamics. The implementation is depicted in fig. 2. From a physical perspective, *one can visualize the kernel embedding of the model's internal activations as a drum membrane and the output as drumstick hitting the membrane during each test cycle.* The resultant modes of membrane vibration (that depend on where exactly the membrane was hit) quantify the uncertainties of the model at various energy levels with respect to the output, which is what we are interested in extracting. We submit various advantages offered by our framework over traditional model uncertainty quantification paradigms.

- Our framework is non-parametric as well as non-intrusive to the model's training process and hence can be implemented universally on trained machine learning models although we restrict ourselves to neural network models in this paper.

- Owing to the established statistical richness of the RKHS, the kernel mean embedding of the model utilizes all even order intrinsic associations of the model’s internal structure (valuable information that is usually ignored in conventional applications).
- We further posit that our framework, which yields high resolution multi-scale uncertainty features, exhibits increased sensitivity towards the characterization of the model’s internal realizations of data and is able to better quantify regions of test data where the model hasn’t been trained, when compared to established methods.

### 1.3 Paper Structure

Further parts of the paper are organized as follows. We begin by introducing the kernel mean embedding (KME) theory in section 2, where we discuss some of its relevant properties. We also introduce the information potential field (IPF) metric as an empirical estimate of the KME and the primary metric used in this paper. We highlight its relevance with respect to Renyi’s entropy. In section 3, we introduce a quantum physical formulation of the data derived from the IPF and show in section 4 how this interpretation opens the doors to a novel uncertainty moment decomposition method, inspired from established methods in quantum physics. Section 5 presents a step-by-step summary of the entire proposed framework. We first analyze our framework from a completely data driven perspective (without involving a model) and provide pedagogical examples in section 6 using implementation of the framework on time-series signals, which provides an intuitive understanding of how it characterizes data dynamics.

We subsequently present the application of the framework for quantifying predictive uncertainties of neural network models in section 7. Related experimental results are provided in section 8 which initially consist of examples illustrating advantages offered by our framework compared to established methods such as Monte Carlo dropout and GP regression. Further results on some benchmark datasets provide quantified evidence demonstrating the same.

## 2 Kernel Mean Embedding

### 2.1 General Definition and Properties

Kernel methods have been very popular and well established in the field of machine learning (Smola & Schölkopf, 1998). The crux of their success is largely owed to a powerful property of the reproducing kernel Hilbert space (RKHS) associated with positive definite kernels called the “kernel trick” (Aronszajn, 1950), which allows one to pose any problem in an input set  $X$  as a linear-algebraic problem in its RKHS,  $H$ , with a non-linear transformation (embedding) of  $X$  into  $H$  induced by a kernel  $k : X \times X \rightarrow R$ . In other words, the RKHS, constructed by an appropriate kernel, allows one to simplify any non-linear relationship in an input space as a linear expression in a higher dimensional space. This property has led to the advent of many popular kernel based algorithms in machine learning (Hofmann et al., 2008; Liu et al., 2011). Following similar intuition, another elegant property of the RKHS is the theory of kernel mean embedding (KME) which allows one to non-parametrically quantify a data distribution from the input space as an element of its associated RKHS (Berlinet &

Thomas-Agnan, 2011). The main idea stems from the probabilistic generalization of the measure-theoretic viewpoint of data. For a detailed explanation of the metric, we refer the reader to (Muandet et al., 2017). Its definition is summarized as follows.

**Definition 1 (Kernel Mean Embedding)** *Suppose that the space  $\mathcal{Z}(\mathcal{X})$  consists of all probability measures  $\mathbb{P}$  on a measurable space  $(\mathcal{X}, \Sigma)$ . The kernel mean embedding of probability measures in  $\mathcal{Z}(\mathcal{X})$  into an RKHS denoted by  $\mathcal{H}$  and characterized with a reproducing kernel  $k : X \times X \rightarrow \mathbb{R}$  is defined by a mapping*

$$\mu : \mathcal{Z}(\mathcal{X}) \rightarrow \mathcal{H}, \quad \mathbb{P} \mapsto \int k(x, \cdot) d\mathbb{P}(x)$$

Hence the kernel mean embedding (KME) represents the probability distribution in terms of a mean function by utilizing the kernel feature map in the space of the distribution. In other words,

$$\phi(\mathbb{P}) = \mu_{\mathbb{P}} = \int k(x, \cdot) d\mathbb{P}(x) \quad (1)$$

There are several useful properties associated with the KME. For instance, it is injective, meaning that  $\mu_{\mathbb{P}} = \mu_{\mathbb{Q}}$  only when  $\mathbb{P} = \mathbb{Q}$ , thus allowing for unique characterizations of data distributions. It also makes minimal assumptions on the data generating process and enables extensions of most learning algorithms in the space of probability distributions.

In this paper, we propose a KME based feature decomposition of data wherein we extract the successive quantum *stochastic energy modes* associated with the data. This is accomplished by reinterpreting the data space as a physical system by utilizing the KME. We reformulate the empirical form of KME in terms of a probabilistic wavefunction metric. In doing so, we treat the space of data as a quantum physical *force field*

composed of inherent uncertainties wherein the interaction of an information particle (data sample) with the field associates an implicit potential energy with the information particle. Thereafter, we extract the various energy modes associated with the information particle from this formulation of data by mimicking established concepts of quantum physics used popularly in the Eigenstate decomposition of physical systems. In order to explain and motivate the physical characterization of the KME, we first describe its empirical estimate and the relevance of the estimate with respect to popular information theoretic measures in the next section before its physical interpretation and uncertainty extraction in sections 4 and 5 respectively.

## 2.2 Empirical Estimate

In most real world applications, there is no information available regarding the nature of  $\mathbb{P}$ . One must therefore resort to empirical estimation of the KME. The simplest method of empirically computing the KME is by computing its unbiased estimate given by

$$\hat{\mu} = \frac{1}{n} \sum_{t=1}^n k(x_t, \cdot). \quad (2)$$

Here  $\hat{\mu}$  converges to  $\mu$  for  $n \rightarrow \infty$ , in concordance with the law of large numbers. One can intuit that the empirical KME is also a result of the general Dirac formulation assigning a mass of  $1/n$  to every data sample. This also gives rise to the interpretation of the empirical KME as an instance of a point process (Muandet et al., 2017).

## 2.3 Relevance in Renyi's Entropy Estimation

Renyi's quadratic entropy (Rényi et al., 1961) is given by

$$H_2(X) = -\log \int p(x)^2 dx = -\log V(X). \quad (3)$$

The argument of the logarithm in Renyi's entropy,  $V(X)$ , is an important quantity called the information potential (IP) of the data set (Principe et al., 2000), which is simply the mean value of the PDF. One can estimate this quantity by using the Parzen density estimator (Parzen, 1962) for estimating  $p(x)$ . Hence, assuming a Gaussian kernel window of kernel width  $\sigma$ , one can readily estimate directly from experimental data  $x_i, i = 1, \dots, N$  the information potential as

$$\begin{aligned} V(X) &= \int p(x)^2 dx = \int \left( \frac{1}{N} \sum_{i=1}^N G_\sigma(x - x_i) \right)^2 dx \\ &= \frac{1}{N^2} \int \left( \sum_{i=1}^N \sum_{j=1}^N G_\sigma(x - x_j) \cdot G_\sigma(x - x_i) \right) dx \\ &= \frac{1}{N^2} \sum_{i=1}^N \sum_{j=1}^N \int G_\sigma(x - x_j) \cdot G_\sigma(x - x_i) dx \\ &= \frac{1}{N^2} \sum_{i=1}^N \sum_{j=1}^N G_{\sigma/\sqrt{2}}(x_j - x_i) \end{aligned} \quad (4)$$

Hence the IP is a number obtained by the double sum of the Gaussian functions centered at differences of samples with a larger kernel size. Exactly the same result is obtained using the empirical estimate of the KME in a RKHS defined by the Gaussian function. There is a physical interpretation of  $V(X)$  if we think of the samples as particles in a potential field, hence the name information potential. It can also be interpreted as the total potential created by the data set in an RKHS, i.e.

$$V(X) = \frac{1}{N} \sum_{j=1}^N V(x_j), \quad (5)$$

where,

$$V(x) = \frac{1}{N} \sum_{i=1}^N G(x - x_i) \quad (6)$$

represents the *field* due to each sample, which can be interpreted as an information particle. We refer to  $V(x)$  as the *information potential field* (IPF) and it is basically a continuous function over the RKHS obtained by the sum of Gaussian bumps centered on the samples. We now delve into the quantum physical interpretation of the empirical KME which we now refer to as the IPF henceforth.

### 3 Quantum Interpretation of the IPF

From a physical perspective, systems are conceptualized as either *classical* or *quantum*. Classical systems are generally characterized by dynamic variables that are smoothly varying and can be modeled by deterministic parameters (Newtonian laws, for instance). Quantum physical systems, on the other hand, are characterized by jumps with increased stochasticity and uncertainty in the measurement of their associated parameters. The composition of probabilistic wave-function modes determines system behavior in this case. The dynamics of a physical particle under the influence of a general quantum system can be described as follows (Griffiths & Schroeter, 2018).

**Definition 2 (General Quantum System)** *The time-independent Schrödinger's equation for a particle at position  $x$  in a general quantum system is given by*

$$\hat{H}\psi = \left( -\frac{\hbar^2}{2m}\nabla^2 + V_r(x) \right) \psi(x) = E\psi \quad (7)$$

where the notations have the following meaning,

- $\hat{H}$  denotes the Hamiltonian operator and is given by  $\hat{H} = -\frac{\hbar^2}{2m}\nabla^2 + V(x)$ , where
  - $-\frac{\hbar^2}{2m}$  is the kinetic energy operator with  $\hbar$  and  $m$  being the Planck's constant and particle mass respectively.
  - $V_r(x)$  represents the potential energy of the particle at position  $x$ .
- $\nabla^2$  is the Laplacian operator.
- $\psi(x)$  is the wave-function value at position  $x$  that also denotes the probability of finding the particle at that position given by  $p(x) = |\psi(x)|^2$ .

A similar interpretation can be extended to data systems as well (Principe, 2010). We can infer that the IPF is always positive and regions of space with more samples will have a larger IP, while regions of the space with few samples will have a lower IP. Here, the shape of the kernel function will determine the “gravity”, instead of the inverse square law of physics. Following this intuition, the idea of a potential field over the space of the samples can be readily extended with quantum theoretical concepts (Principe, 2010). A Schrödinger's time-independent equation equivalent to (7) was formulated to define a new potential energy function  $V_s(x)$  (data-equivalent form of  $V_r(X)$  in (7)) based on a wave-function defined by using the IPF as the probability measure  $p(x)$ . Since  $p(x) = |\psi(x)|^2$ , then for a set of information particles with a Gaussian kernel, the wave-function for one dimensional information particle becomes,

$$\psi(x) = \sqrt{\frac{1}{N} \sum_{i=1}^N G_\sigma(x - x_i)} \quad (8)$$

Furthermore, we can assume  $m = 1$  in (7) since all information particles are assumed to have the same mass. We can also rescale  $V_s(x)$  such that  $\sigma$  (bandwidth of the kernel



window) is the only free parameter that replaces all physical constants. This reformulates (7) to yield the Schrödinger's time-independent equation for information particles as

$$H\psi(x) = \left( -\frac{\sigma^2}{2}\nabla^2 + V_s(x) \right)\psi(x) = E\psi(x) \quad (9)$$

where  $H$  denoted the Hamiltonian. Solving for  $V_s(x)$ , we obtain:

$$V_s(x) = E + \frac{\sigma^2/2\nabla^2\psi(x)}{\psi(x)} \quad (10)$$

which was called the *quantum information potential field* (QIPF) denoted by  $V_s(x)$ . To determine the value of  $V_s(x)$  uniquely, we require that  $\min(V_s(x)) = 0$ , which makes

$$E = -\min \frac{\sigma^2/2\nabla^2\psi(x)}{\psi(x)} \quad (11)$$

where  $0 \leq E \leq 1/2$ . Note that  $\psi(x)$  is the eigenfunction of  $H$  and  $E$  is the lowest eigenvalue of the operator, which corresponds to the ground state. Given the data set, we expect  $V_s(x)$  to increase quadratically outside the data region and to exhibit local minima associated with the locations of highest sample density (clusters). This can be interpreted as clustering since the potential function attracts the data distribution function  $\psi(x)$  to its minima, while the Laplacian drives it away, producing a complicated potential function in the space. We should remark that, in this framework,  $E$  sets the scale at which the minima are observed. This derivation can be easily extended to multidimensional data. We can see that  $V_s(x)$  in (10) is also a potential function that differs from  $V(x)$  in (6) because it is now an energy based formulation associated with the quantum description of the IPF.

## 4 Extraction of QIPF Energy Modes

Unlike the classical interpretation, the quantum interpretation provides a much more detailed decomposition of the system dynamics by assuming it to consist of a large (potentially infinite) number of stochastic *features*, given by the energy modes. Likewise, when applying this quantum field potential to data, the same interpretation holds. Because of the finite number of samples, the local structure of the PDF in the space of samples will be very difficult to quantify. In the input space, we normally use clustering or other techniques to achieve this goal, but we still have an enormous difficulty in characterizing the tails of distributions. Here it is relevant to remember the characteristic function of the PDF and the cumulants, which has been a work horse of statistics. The issue with the cumulants is the complexity of estimating the higher order moments in high dimensional data. Here, instead, we will follow the teachings of quantum theory and will employ a model decomposition of the wave function to subsequently extract uncertainty modes that focus on characterizing the tail regions of the data PDF. We first analyze the behavior of the quantum harmonic oscillator, a popular example of a quantum model that is pervasively used in many fields to describe system behavior (economics, for instance (Meng et al., 2016; Ahn et al., 2018)). The following definition describes the extraction of the system's wave-function modes (Griffiths & Schroeter, 2018).

**Definition 3 (Quantum Harmonic Oscillator)** *The potential energy of a particle can be generalized using Hooke's law as  $V(X) = \frac{1}{2}m\omega^2x^2$ . The Hamiltonian of the particle*

characterizes its dynamic parameters (position and momentum) and is formulated as

$$\hat{H} = \frac{\hat{p}^2}{2m} + \frac{1}{2}m\omega^2 x^2 \quad (12)$$

where  $\omega = \sqrt{\frac{k}{m}}$  is the angular frequency of the oscillator,  $x$  is the position and  $\hat{p} = -i\hbar\frac{d}{dx}$  represents the momentum operator. Given this Hamiltonian, the time-independent Schrödinger's equation can be formulated as

$$\hat{H}\psi(x) = \left[ -\frac{\hbar^2}{2m} \frac{d^2}{dx^2} + \frac{1}{2}m\omega^2 x^2 \right] \psi(x) = E\psi(x) \quad (13)$$

This differential equation can be treated as an eigenvalue problem and solved using the spectral method to yield a family of wave-function modes,  $\psi_n(x)$ , that amount to successive Hermite polynomial moments. The solutions are given as:

$$\begin{aligned} E_0 &= \frac{\hbar\omega}{2}, & \psi_0 &= \alpha_0 e^{-\frac{y^2}{2}} \\ E_1 &= \frac{3\hbar\omega}{2}, & \psi_1 &= \alpha_0 (2y) e^{-\frac{y^2}{2}} \\ E_2 &= \frac{5\hbar\omega}{2}, & \psi_2 &= \alpha_0 (4y^2 - 2) e^{-\frac{y^2}{2}} \end{aligned} \quad (14)$$

Here,  $y = \sqrt{\frac{m\omega}{\hbar}}x$ ,  $\psi_0, \psi_1, \psi_2 \dots$  are the obtained wave-function modes and  $E_0, E_1, E_2 \dots$  are their corresponding eigenvalues. Therefore the solution to the Schrödinger equation for the harmonic oscillator yields infinite eigenfunctions successively associated with each other through Hermite polynomials.

Hence we see that the quantum interpretation enables one to extract the various intrinsic energy modes associated with the system, along with the corresponding eigenvalue of each mode. In the previous section, we have described the Schrödinger's equation associated with the quantum IPF (QIPF) given by (9) which essentially provides a quantum

interpretation of data dynamics similar to how (13) does for the harmonic oscillator. Our goal is to now extract successive energy modes (analogical to those obtained in (14)) associated with the QIPF given by  $V_s(x) = E + \frac{\sigma^2/2\nabla^2\psi(x)}{\psi(x)}$ . The ground state of the wave-function, in the case of the QIPF formulation, has already been probabilistically defined as an expression of the empirical KME given by  $\psi(t) = \sqrt{p(t)} = \sqrt{\frac{1}{n} \sum_{i=1}^n k(x_i, t)}$ . We use this information to summarize the QIPF state extraction procedure in the following conjecture.

**Conjecture 1 (Extraction of QIPF Energy Modes)** *Consider the QIPF of the data samples  $x$  as  $V_s(x) = E + \frac{\sigma^2/2\nabla^2\psi(x)}{\psi(x)}$  with the associated ground state wave-function given by  $\psi(x) = \sqrt{\frac{1}{n} \sum_{i=1}^n k(x_i, t)}$ . The approximate higher order energy modes of  $\psi(x)$  can be extracted by projecting the ground state wave-function into the corresponding order Hermite polynomial given by  $\psi_k(x) = H_k^*(\psi(x))$ , where  $H_k^*$  denotes the normalized  $k^{\text{th}}$  order Hermite polynomial, normalized so that  $H_k^* = \int_{x=-\infty}^{\infty} e^{-x^2} [H_k(x)]^2 dx =$*

1. This leads to the evaluation of the higher order QIPF states as

$$\begin{aligned} V_s^k(x) &= E_k + \frac{\sigma^2/2\nabla^2 H_k^*(\psi(x))}{H_k^*(\psi(x))} \\ &= E_k + \frac{\sigma^2/2\nabla^2 \psi_k(x)}{\psi_k(x)} \end{aligned} \tag{15}$$

where  $k$  denotes the order number and  $E_k$  denotes the corresponding eigenvalues of the various modes and is given by

$$E_k = -\min \frac{\sigma^2/2\nabla^2 \psi_k(x)}{\psi_k(x)} \tag{16}$$

The extracted modes of the data QIPF given by  $V_s^k(x)$  are thus stochastic functionals depicting the different moments of *potential energy* of the data at any point  $x$ . This

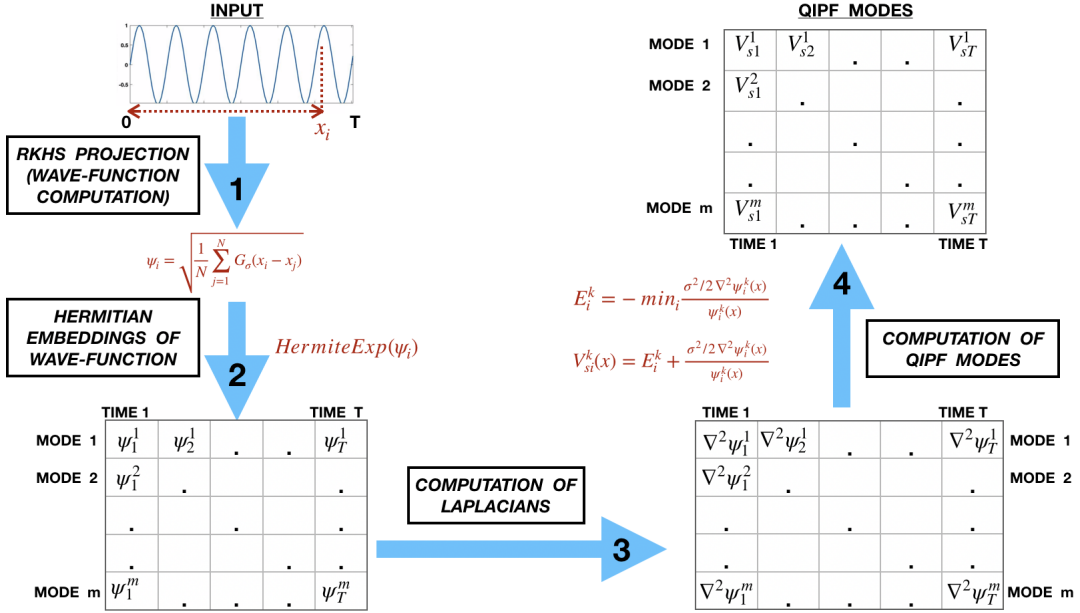


Figure 3: Proposed framework for extraction of quantum uncertainty states

is different from the IPF formulation of (6) because  $V_s^k(x)$  is an energy based metric resembling the potential energy operator in a quantum harmonic oscillator at various energy levels (Eigenstates) depicted by  $E_k$ .

## 5 Summarizing the Framework

The key aspects of the framework are summarized as follows.

- **Metric Construction:** We construct an RKHS based metric space of the data using the kernel mean embedding function which provides a non-parametric characterization of the implicit PDF of the data without making any prior assumptions.
- **Quantum-Physical Interpretation:** We use the empirical KME (or the IPF) to define a probabilistic wave-function over the space of data thereby providing a quantum-physical interpretation of data spaces. Thereafter, we utilize the

Schrödinger's equation to provide an energy based interpretation of the data dynamics by imposing kinetic and potential energy operators that are 'stochasticized' by the wave-function over the data metric space, thereby defining the overall energy composition of the data.

- **Potential Energy Expression (QIPF):** We replace all physical constants related to the kinetic energy operator using the kernel bandwidth and thereafter express the potential energy of data, given by the QIPF, as a function of all other terms - eigenvalue, wave-function and the kernel bandwidth. The eigenvalue is simply determined to be a lower bound value which constraints the QIPF to always be positive.
- **Extraction of QIPF States:** We extract approximate energy moments (or modes) of the data QIPF by implementing orthogonal Hermite polynomial projections of the ground state wave-function and finding the corresponding QIPF state.

The implementation details of the framework are illustrated in figure 3.

## 6 Mode Decomposition of Time Series

We begin our analysis of the proposed framework by studying how it characterizes time series signals. We used MATLAB R2019a to obtain the results shown in this section. For an intuitive understanding of how the different QIPF modes get configured in the space of data, we extracted the first 6 modes of a simple sine wave signal. We generated 3000 samples of a 50 Hz unweighted sine wave signal sampled at the rate of 6000 samples per second to mimic a continuous signal. The signal was also normalized

to zero mean and unit standard deviation. We used all 3000 samples as centers to construct the wave-function given by (8) and then evaluated it at each point in the data space range  $x = (-6, 6)$  using a step size of 0.1. We then evaluated the Hermite projections of the wave-function value at each point to subsequently extract 6 QIPF modes using the formulation given by (15). This was done for four different kernel widths whose corresponding QIPF plots (represented by solid color lines) are shown in fig. 4. The dashed line represents the empirical KME estimate (or simply the IP) given by  $p(x) = \psi^2(x) = \frac{1}{N} \sum_{i=1}^N \kappa(x, x_i)$ , which basically gives an estimate of the data PDF. All plots were normalized for easier visualization. Perhaps the most important property of the extracted QIPF modes that can be observed from the plots is that, for all kernel widths, they systematically signify the more uncertain regions of the data space closer to the tails of the data PDF. In fact, one can observe the significant increase in the density (or clustering) of the extracted QIPF modes as one moves farther away from the mean ( $x = 0$ ) and towards the PDF tails. Furthermore, we observe here that the modes appear sequentially based on their orders, with the lower order modes signifying regions closer to the mean and the higher order modes clustering together at the PDF tails. An interesting observation that must also be noted is that, for larger kernel widths (1.8 and 2.6), which exceed the dynamic range of the signal, we can see that some high order modes begin to emerge in the region around the mean. This behavior is remarkably similar to physical systems. If we consider the same drum membrane analogy we used in section I, one can visualize the space of the samples here as the membrane. If we increase the tension of the membrane and hit it, the drum will vibrate for a long time. In our potential field, the stiffness is controlled by the kernel size. If the kernel size

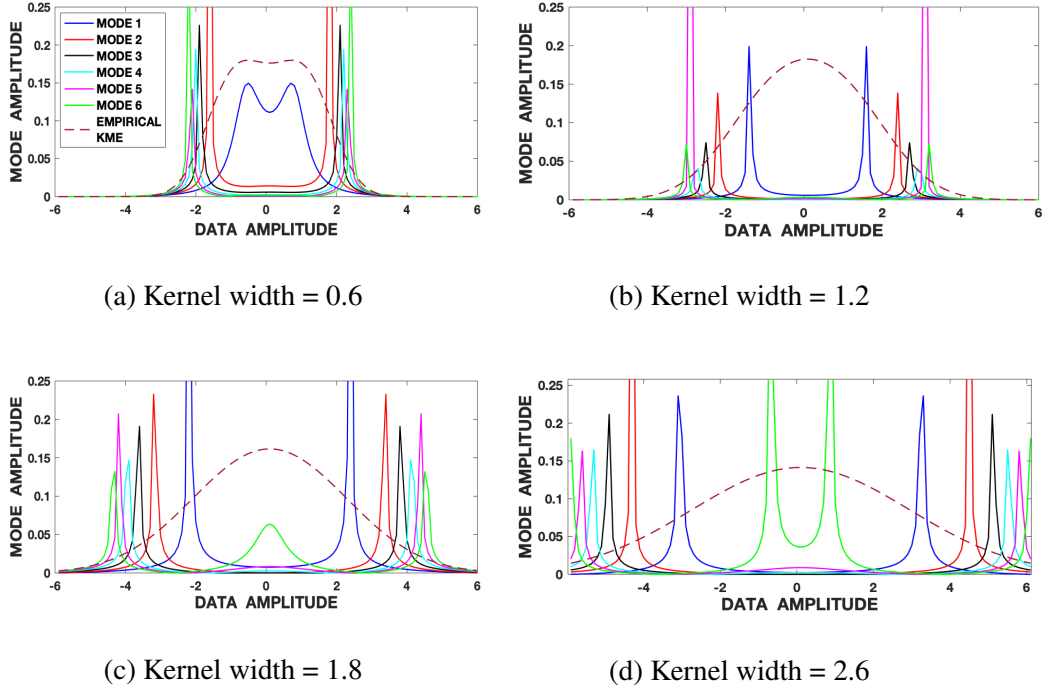


Figure 4: Analysis of mode locations in the data space using different kernel widths. Solid colored lines represent the different QIPF modes. Dashed line represents the empirical KME (IP).

is large, the QIPF becomes stiffer leading to the energy in the higher QIPF modes to increase. If one decreases the kernel size, the membrane becomes more elastic leading to many local modes that decay much faster.

As a pedagogical demonstration to understand how the framework characterizes different dynamical data structures, we implement it to compare the extracted uncertainty modes of a simple sine wave oscillator and a Lorenz series. The sine wave represents one of the simplest time series with a single generating function. The Lorenz series on the other hand is a chaotic deterministic dynamical system with complex state space defined by the following mutually coupled differential equations (with  $\sigma$ ,  $\rho$  and  $\beta$  as



system parameters) governing its dynamics:

$$\frac{dx}{dt} = \sigma(y - x), \quad \frac{dy}{dt} = x(\rho - z) - y, \quad \frac{dz}{dt} = xy - \beta z. \quad (17)$$

We generated 3000 samples of Lorenz series after setting the parameters as  $\sigma = 10$ ,  $\rho = 28$  and  $\beta = 8/3$  and the initial conditions as  $x_1 = 0$ ,  $y_1 = 1$  and  $z_1 = 1.05$ . The signal was also normalized to zero mean and unit variance. We generated two sine wave signals with the first one having a fundamental frequency of 150 Hz and the second one with an added odd harmonic frequency component (150 Hz + 250 Hz). The signals were sampled at a rate of 6000 samples per second and were normalized to zero mean and unit variance. We extracted the first 10 QIPF modes using (15) and (16) to encode the different signals. The kernel width used for doing so was fixed to a moderate value of 1.2 for all signals. Fig. 5 shows the signals (top row) and the corresponding histogram plots (bottom row) of the number of times the value of each QIPF mode dominated over the others throughout the durations of the signals. As can be seen in fig. 5(a), there are only two dominant modes in case of the single frequency sine wave (modes 2 and 3). Addition of an odd harmonic leads to increase in the number of modes contributing to the signal dynamics to four (fig. 5(b)). The dominant modes in the case of Lorenz series, on the other hand, are more spread out (across all 10 modes) thus indicating a more complex data dynamical structure. These trends are quite similar to what we would expect from a frequency decomposition of the signals, except that here we are able to perform this decomposition on a sample-by-sample basis.

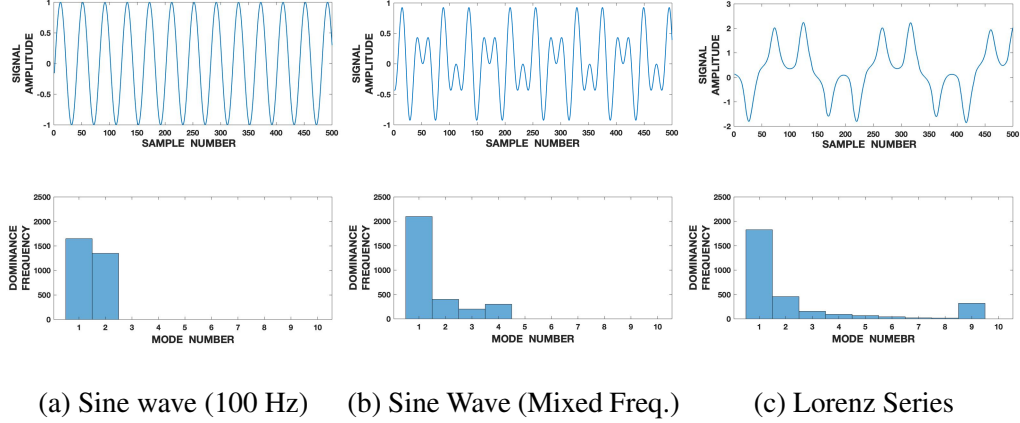


Figure 5: *Top row*: Generated signals from different dynamical systems. *Bottom row*: Dominance frequencies of QIPF states corresponding to each signal.

## 7 Model Uncertainty Quantification

The QIPF mode extraction framework can so be naturally extended for implementation on machine learning models. The fundamental idea here is to create a continuous surrogate embedding of the trained model that represents its intrinsic distribution. We can then extract the QIPF uncertainty modes associated with the interactions between model’s embedding and its output. We expect this to quantify the extent to which the prediction falls within the scope of the model’s intrinsic distribution. As evidenced in the previous section, we expect higher order QIPF modes to cluster in data regions where the model has not been trained, represented by the tails of the input-output mapping PDF learnt by the network, thereby providing a sensitive uncertainty characterization of data spaces unknown to the model. In this regard, we specifically focus on neural network models due to a recent surge in its research interest.

The basic implementation strategy of the QIPF decomposition framework on a trained neural network is the same as the data-based implementation, except for the

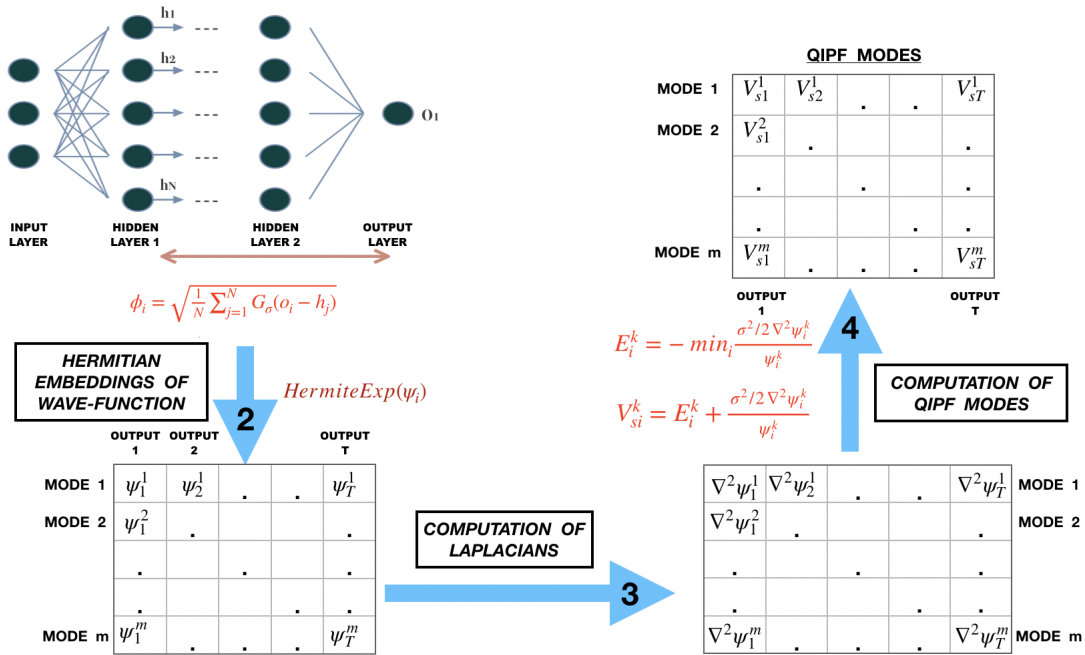


Figure 6: Implementation of the proposed framework on ANN

way in which we construct the information potential field (IPF). In this case, we aim to decompose the interactions between the RKHS fields of different pairs of network layers (with one of them typically being the output layer), thereby obtaining a multi-scale uncertainty representation of the implicit mapping between them. Intuitively, this quantifies the *probabilistic discrepancies* between two layers of the network during each test cycle. The RKHS field of each layer is represented by the kernel feature map constructed by its corresponding node activation outputs. We evaluate the *cross information potential* (CIP) which measures interactions between two information potentials (Principe, 2010). One can represent the cross information potential between two layers of the neural network using a generalized form of the kernel mean embedding formulation. Let us consider two layers of an ANN whose node outputs are represented by the random variables  $L_1$  and  $L_2$ . The kernel feature map of  $L_1$  can then be represented in

the same form as (1) as

$$\mu_{\mathbb{P}_{L_1}} = \int \kappa(l_1, \cdot) \mathbb{P}_{L_1}(l_1) dl_1. \quad (18)$$

The mean evaluation of  $\mu_{L_1}$  at all points specified by  $L_2$  is the cross information potential between  $L_1$  and  $L_2$  and can be represented as

$$\mu_{\mathbb{P}_{L_1}}(\mathbb{P}_{L_2}) = V_c(\mathbb{P}_{L_1}, \mathbb{P}_{L_2}) = \int \int \kappa(l_1, l_2) \mathbb{P}_{L_1}(l_1) \mathbb{P}_{L_2}(l_2) dl_1 dl_2. \quad (19)$$

The empirical evaluation of (19) leads to

$$\hat{V}_c(\mathbb{P}_{L_1}, \mathbb{P}_{L_2}) = \frac{1}{nm} \sum_{i=1}^n \sum_{j=1}^m \kappa(l_1(i) - l_2(j)) \quad (20)$$

The quantum decomposition can then be performed in the same way as before (summarized in fig. 6), thus leading to extraction of multi-scale uncertainty features associated with the layer-layer interactions of the neural network. We will typically consider  $L_2$  to be the output layer in most empirical evaluations, thus measuring the probabilistic interactions between the model’s output and one or more of the hidden layers. Here we will show results with respect to the field created by the hidden layer output thereby finding out uncertainties in the output layer parameters. Since we expect the QIPF modes (resulting from the information potential interactions between the hidden layers and the output) to be more densely clustered in test data regions unknown to the model, we quantify uncertainty ranges associated with the model’s predictions by measuring the standard deviation of QIPF states extracted at each instance of testing.

## 8 Experiments and Analysis

We present simulation results to illustrate and compare performance of the QIPF framework with respect to currently popular approaches for the problem of predictive uncer-

tainty quantification. All simulations described in this section were performed using python 3.6. Being a kernel based approach, we compare the QIPF framework’s performance with that of Gaussian process regression (GPR) (Rasmussen, 2003) which is a widely famed kernel method for machine learning that is known for providing reliable uncertainty estimates associated with its predictions. We also provide comparisons with Monte Carlo dropout (Gal & Ghahramani, 2016) that has gained recent popularity as an approximate variational inference based method for uncertainty quantification of neural networks.

## 8.1 Regression

### Datasets

We generate two different regression datasets as didactic examples for experimental comparisons and analysis. The idea of such datasets is to simulate real world scenarios where tasks in machine learning encounter test data from outside the training domain or have to face external noise or outliers in their training set. Indeed these synthesized datasets have also been used in various uncertainty quantification literature for demonstration of methods (Osband et al., 2016b; Gal & Ghahramani, 2016). The first dataset consists of 60 regression pairs  $x_i, y_i$  from the following weighted sine signal:

$$y_i = x_i \sin(x_i). \tag{21}$$

Here, the training inputs  $x_i$  are drawn uniformly from  $(-5, 5)$ . The dataset is shown in fig. 7a as synthesized dataset I. The blue circles represent the training samples and the red dotted line represents its underlying governing function in the region  $(-15, 15)$ .

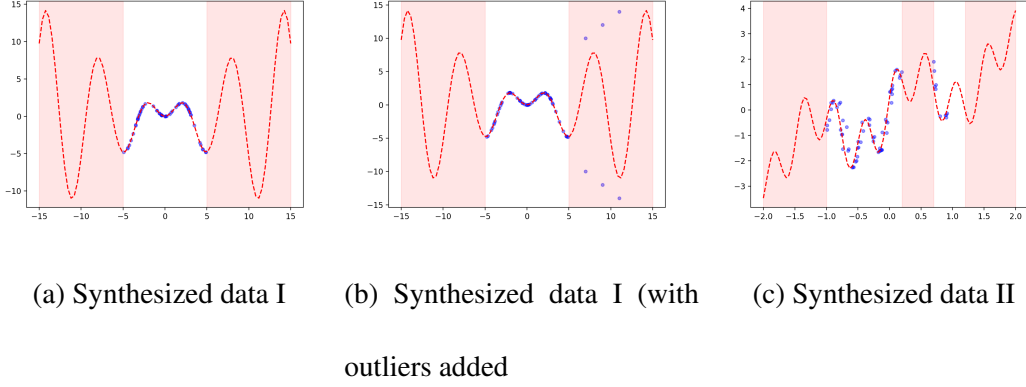


Figure 7: Synthesized datasets for experimental evaluations. Blue circles depict the sampled training data and red dashed lines represent their associated generating functions. Pink bands represent regions with no training samples.

Although the training pairs are sampled only from a specific region, testing (for all algorithms) is performed in the entire data region by sampling 120 test data pairs uniformly from the region  $(-15, 15)$ . The pink bands represent test data regions for which training data has not been provided. We therefore expect high predictive uncertainties in these regions. As part of the analysis, we also add 6 widely varying outlier samples (not lying on the governing function) to the training set of synthesized dataset I as shown in fig. 7b. Synthesized data II consists of noisy regression pairs  $x_i, y_i$  sampled from the following signal:

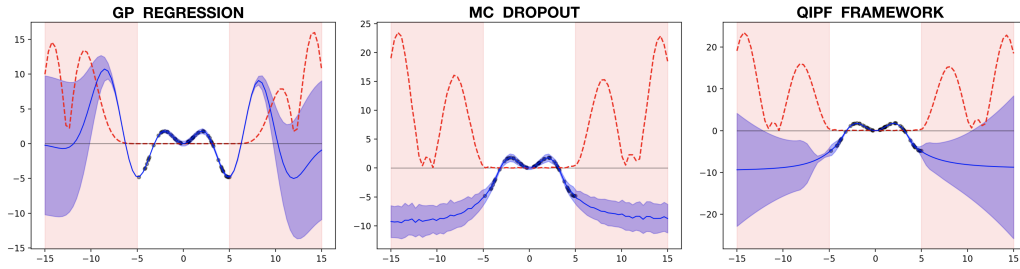
$$y_i = x_i + \sin(\alpha(x_i + w_i)) + \sin(\beta(x_i + w_i)) + w_i. \quad (22)$$

Here, we set  $\alpha = 4$ ,  $\beta = 13$  and  $w_i \sim N(\mu = 0, \sigma^2 = 0.03^2)$ . We draw 40 input samples for training uniformly from  $(-1, 0.2)$  and 10 from  $(0.7, 1)$ , leaving the region  $(0.2, 0.7)$  as blank. For model testing, we draw 120 test sample pairs uniformly from  $(-2, 2)$ . The dataset is depicted in fig 7c. In addition to these datasets, we also perform model extrapolation experiments on the Mauna Loa CO2 dataset which consists

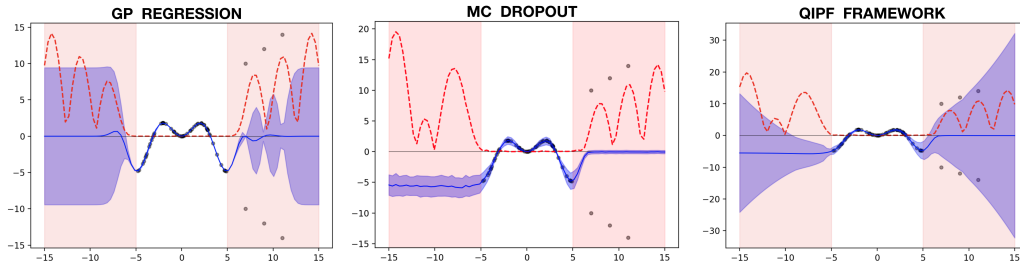
of atmospheric CO<sub>2</sub> concentrations measured from in situ air samples collected at the Mauna Loa Observatory, Hawaii (Keeling & Whorf, 1991).

### **Model Implementations**

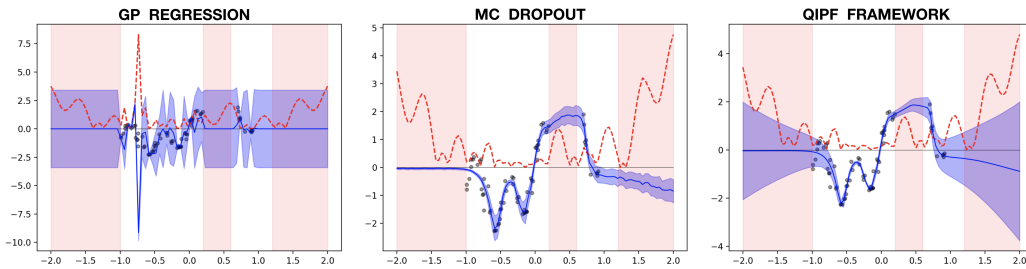
For implementing the MC dropout and QIPF framework on synthesized data I, we use a small fully connected and ReLU activated neural network with 3 hidden layers containing 20 neurons each. We train the network on the given training samples in the region  $(-5, 5)$ . Since the network is very small, the dropout rate for training was set to 0.05 (similar to that recommended in (Gal & Ghahramani, 2016) for a similar network size) and we used 100 epochs with the batch size equal to the number of training samples. Thereafter we tested the network on 120 input points sampled uniformly from the entire data region  $(-15, 15)$ . For implementing MC dropout, the test dropout rate was set to 0.2 and we used 100 forward stochastic runs to quantify the uncertainty interval at each test point. We implemented the QIPF framework by extracting 5 cross-QIPF states of the prediction point with respect to the activation outputs of each hidden layer. We used a kernel width based on the values of hidden layer activation outputs and fixed it to 20 times the Silverman's thumb rule for bandwidth estimation (Silverman, 2018). The criteria for kernel width depends on the range of data space on which the QIPF framework is to be implemented as well as the desired resolution of modes. Since we are operating on a relatively small neural network over a limited data span, we speculated that 5 QIPF modes would be enough for our implementation. Thereafter we quantified the uncertainty interval by measuring the standard deviation of the extracted cross-QIPF states at each point of prediction. For synthesized data II, we used a 2-layer network with 50



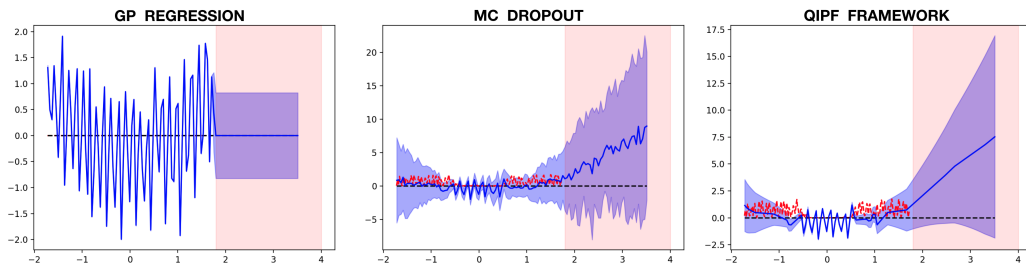
(a) Synthesized data - I



(b) Synthesized data - I (with outliers added)



(c) Synthesized data - II



(d) Mauna Loa CO2 data

Figure 8: Comparison of the different predictive UQ methods. Blue lines represent model predictions. Blue shaded areas represent their associated uncertainty ranges. Red dotted lines are test prediction errors. Pink bands represent untrained regions.



neurons each for training. The training dropout rate was set to 0.1 and we used 100 training epochs with the batch size equal to the total training data. We implemented MC dropout and QIPF frameworks in the same manner as before on the entire data region  $(-2, 2)$  using 120 uniformly generated test samples. In the case of the CO2 data, we used a relatively larger fully connected ReLu network of 5 layers with 100 neurons each. Training dropout rate in this case was set as 0.2. We test the network over the entire training region as well as an extrapolated region outside of the it. We also fitted the Gaussian Process regression model on all datasets. In each case, the parameters associated with the covariance kernel function were chosen using grid search so as to maximize the log marginal likelihood of the data.

### **Analysis of Results**

The results of the different uncertainty quantifiers are shown in fig. 8. The blue line represents the predictions and the blue shaded regions depict the uncertainty ranges (standard deviation) at the prediction points quantified by the different methods (GPR, MC dropout and QIPF). Red dotted line indicates the test set prediction errors with respect to the generating function values at those points and the pink bands represent regions in the input space where no training samples were generated. For synthesized data I in fig. 8a, it can be observed that the GP regression model is able to better identify the generating signal dynamics than the neural network, producing low predictive errors for some distance outside of the training set. This is expected for small non-linear datasets where kernel methods outperform ANNs. It also produces well calibrated uncertainty ranges that are seen to be roughly proportional to the predictive errors. The QIPF framework

can also be seen to produce uncertainty ranges that scale more proportionally with respect to the test error. MC dropout, on the other hand, produces comparatively less realistic uncertainties that soon converge to a constant level showing no change with respect to prediction errors thereafter. We observe wide disparities between the uncertainty quantification of the three algorithms in fig. 8b when the outliers are added to the training data (synthesized data I). We observe here that all models converge to the center of the outlier data when making predictions at those points. This is expected since the mean of such widely varying data points would represent the lowest error region for most learning models. However, we also notice that MC dropout becomes very overconfident with low uncertainties associated with its predictions at the outlier regions, which is opposite of what we would ideally expect. This is also reported in (Hernández-Lobato & Adams, 2015). GP regression model also shows unrealistically low uncertainties in its predictions at the particular outlier points though it still produces increased uncertainty range around them. Also, unlike before, the GP model can be observed to converge to an unrealistic constant level of uncertainty as one goes outside of the training region, regardless of the increase in predictive errors. The QIPF framework, on the other hand, shows a remarkable property of *increasing* its uncertainty range at the outlier regions, which is the ideal behavior. It is also seen to maintain its property of increasing proportionally with the predictive errors in all outside data regions. This indicates the sensitivity of the QIPF framework towards data variances and outliers in the training set. For synthesized data II (which consists of added normal noise), similar observations can be made related to the nature of uncertainties quantified by the different methods outside of the training domain. As before, the QIPF framework is seen to

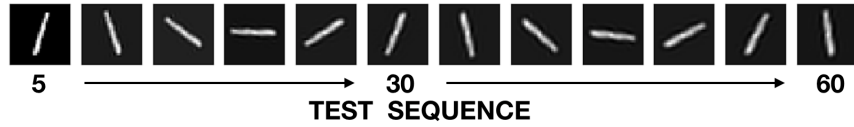
produce uncertainty estimates that increase more realistically outside the training domain and more proportional to the predictive errors when compared to MC dropout and GP regression. Both QIPF framework and MC dropout can be seen to be sensitive in their characterizations of uncertainty in the thin middle untrained band (given by the region  $(0.2, 0.7)$ ). However, we also observe here that, like before, MC dropout becomes unrealistically overconfident due to large variances in the training data pairs (on the left side of its corresponding graph in fig. 8c). Similar analysis on the CO<sub>2</sub> data (fig. 8d) reveals GP regression to fit better than the other two models in the training region with very little error. However, it continues to be insensitive to predictive error outside the training domain by exhibiting a constant level of uncertainty when extrapolated during testing. The same trend of GP regression is reported in (Gal & Ghahramani, 2016). Both MC dropout and QIPF framework extrapolate more realistically in terms of uncertainty. We summarize the observations related to the QIPF framework from these results as follows.

- The framework is observed to be robust towards training set outliers and is able to effectively capture the model's associated uncertainties with respect to them during testing. This can be attributed to the ability of the Gaussian RKHS in better capturing the true data distributions.
- For all datasets, the QIPF framework is observed to produce uncertainty estimates that are more consistent with predictive errors in all regions of the data domain consequently exhibiting realistic uncertainty ranges for both model interpolation and extrapolation applications.

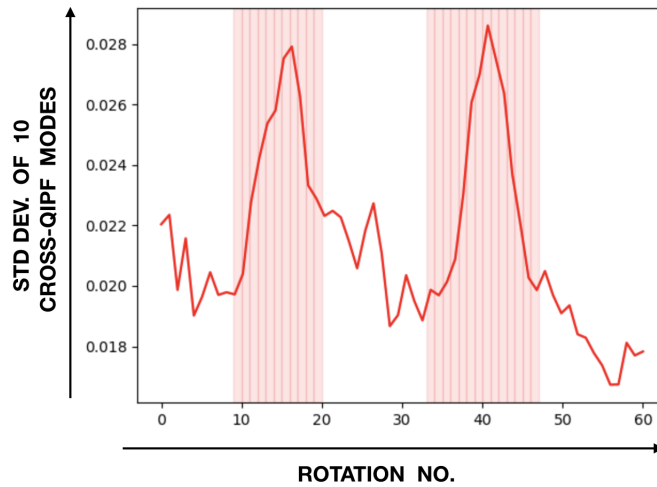
- The framework also exhibits increased sensitivity towards inherent data variances.

## 8.2 Classification

We also demonstrate the ability of the QIPF framework quantify uncertainties related to classification problems. Towards this end, we train a ReLu activated and fully connected MLP with 3 hidden layers with 512 - 256 - 128 neurons respectively (from first to last hidden layers) on the MNIST dataset (LeCun et al., 1998). We train the network without the implementation of dropout for 10 epochs using a batch size of 100. During testing, we rotated a single digit of 1 gradually (60 times uniformly) and fed each rotated version to the trained NN. During each test instance, we extracted the first 10 cross QIPF modes



(a) Testing sequence obtained by rotating MNIST digit of one.



(b) Uncertainty results of QIPF framework tested on rotated sequence of a digit.

Figure 9: Behavior of QIPF framework towards classification errors (pink bands)

of the average node input value of the last layer (before thresholding) with respect to the activation outputs of hidden layer 1. In this application, we extracted the QIPF modes twice using different kernel widths (20x and 30x the Silverman bandwidth of the hidden layer 1 activation outputs) and considered the average of the two runs. This was done to ensure that the modes cover the range between the first and last hidden layer outputs. Fig. 9a shows samples of the gradually rotated test sequence and fig. 9b shows the graph of the standard deviation of the 10 average QIPF modes at each test input. The pink bands represent the rotations at which the network produced incorrect classification results. One can observe the sharp rise of the standard deviation of the uncertainty modes at the misclassified test regions thus indicating that the framework produces uncertainty results consistent with the model classification errors.

### **8.3 Benchmark Datasets**

We quantify and compare the quality of uncertainty estimates of our method with MC dropout over UCI datasets that are typically used as benchmarking data in various uncertainty quantification literature. We measure the quality of uncertainty estimate by quantifying how calibrated the uncertainty estimates are with respect to prediction errors. We chose datasets with diverse numbers of samples in order to test the framework on different forms of non-linearities. We train neural networks with 50 neurons in each hidden layer on 20 randomly generated train-test splits of the normalized UCI datasets (similar to the experimental framework of (Gal & Ghahramani, 2016; Hernández-Lobato & Adams, 2015)). A single kernel width of 1 was used in this case for extracting 10 QIPF states. We measured the RMSE of the uncertainty range (std. deviation of the QIPF

UCI Datasets	N	Q	MC Dropout	QIPF
Yatch Hydrodynamics	308	6	0.332 +- 0.051	<b>0.204 +- 0.050</b>
Boston housing	506	13	0.246 +- 0.038	<b>0.234 +- 0.042</b>
Power Plant	9568	4	0.170 +- 0.035	<b>0.124 +- 0.035</b>
Concrete Strength	1030	8	0.234 +- 0.035	<b>0.221 +- 0.044</b>
Energy Efficiency	768	8	0.238 +- 0.028	0.268 +- 0.061

(a) 1-hidden layer NN

Yatch Hydrodynamics	308	6	0.294 +- 0.093	<b>0.169 +- 0.046</b>
Boston housing	506	13	0.222 +- 0.041	0.234 +- 0.049
Power Plant	9568	4	0.151 +- 0.050	<b>0.150 +- 0.057</b>
Concrete Strength	1030	8	0.218 +- 0.036	<b>0.211 +- 0.043</b>
Energy Efficiency	768	8	0.235 +- 0.032	0.274 +- 0.046

(b) 2-hidden layer NN

Yatch Hydrodynamics	308	6	0.226 +- 0.063	<b>0.167 +- 0.038</b>
Boston housing	506	13	0.223 +- 0.023	0.234 +- 0.041
Power Plant	9568	4	0.146 +- 0.038	<b>0.144 +- 0.05</b>
Concrete Strength	1030	8	0.220 +- 0.030	<b>0.204 +- 0.035</b>
Energy Efficiency	768	8	0.263 +- 0.034	<b>0.240 +- 0.048</b>

(c) 3-hidden layer NN

Table 1: Normalized RMSE between the standard deviation of quantified uncertainty and the test error. **N** denotes the number of samples and **Q** denotes data dimensionality.

modes at each test sample) with respect to the test error in each train-test split. This was done to measure how calibrated and scaled the estimated uncertainty range was with respect to the error. The average RMSE as well as its standard deviation for the 20 test splits are presented in table 1 for the framework’s implementation on neural network architectures consisting of 1, 2 and 3 hidden layers respectively. It can be observed that the QIPF framework has lower RMSE values than MC dropout for most datasets in all network configurations thereby indicating that the estimated uncertainty using QIPF is more realistic.

## **Conclusion**

In this paper, we introduced a new information theoretic approach for quantifying uncertainty that is inspired by quantum physical principles and concepts. We formulated a new moment decomposition framework for data by utilizing the RKHS based metric called the information potential field. The key advantages offered by our framework are its non-parametric nature, ability to be implemented on a sample-by-sample basis and its sensitivity towards unseen data or model regions. We gave pedagogical examples to show how our model provides a multi-scale characterization of the tails of the data PDF about which we generally have the least amount of information. We demonstrated how our framework can be utilized as a powerful tool for the predictive uncertainty quantification of models in both regression and classification tasks. Related results indicate that our framework is able to recognize and quantify training outlier regions of the data encountered during model testing, unlike MC dropout or GP regression. It is also able

to more appropriately remain consistent with respect to the predictive errors.

In the future, we intend to conduct more data-based implementations of the framework in order to explore its utility in the signal processing domain.

## Acknowledgments

We would like to acknowledge the support provided for this work by DARPA under agreement number HR001116S0001.

## References

- Ahn, K., Choi, M., Dai, B., Sohn, S., & Yang, B. (2018). Modeling stock return distributions with a quantum harmonic oscillator. *EPL (Europhysics Letters)*, *120*(3), 38003.
- Aronszajn, N. (1950). Theory of reproducing kernels. *Transactions of the American mathematical society*, *68*(3), 337–404.
- Bergman, S. (1970). *The kernel function and conformal mapping* (Vol. 5). American Mathematical Soc.
- Berlinet, A., & Thomas-Agnan, C. (2011). *Reproducing kernel hilbert spaces in probability and statistics*. Springer Science & Business Media.
- Bishop, C. M. (1995). Bayesian methods for neural networks.



- Boltzmann, L. (1877). *Über die beziehung zwischen dem zweiten hauptsatze des mechanischen wärmetheorie und der wahrscheinlichkeitsrechnung, respective den sätzen über das wärmeleichgewicht*. Kk Hof-und Staatsdruckerei.
- Fang, K.-T., Li, R., & Sudjianto, A. (2005). *Design and modeling for computer experiments*. Chapman and Hall/CRC.
- Fisher, R. A. (1922). On the mathematical foundations of theoretical statistics. *Philosophical Transactions of the Royal Society of London. Series A, Containing Papers of a Mathematical or Physical Character*, 222(594-604), 309–368.
- Forrester, A., Sobester, A., & Keane, A. (2008). *Engineering design via surrogate modelling: a practical guide*. John Wiley & Sons.
- Frieden, B. R. (2004). *Science from fisher information: a unification*. Cambridge University Press.
- Frieden, B. R., & Hawkins, R. J. (2010). Quantifying system order for full and partial coarse graining. *Physical Review E*, 82(6), 066117.
- Gal, Y., & Ghahramani, Z. (2016). Dropout as a bayesian approximation: Representing model uncertainty in deep learning. In *international conference on machine learning* (pp. 1050–1059).
- Graves, A. (2011). Practical variational inference for neural networks. In *Advances in neural information processing systems* (pp. 2348–2356).
- Griffiths, D. J., & Schroeter, D. F. (2018). *Introduction to quantum mechanics*. Cambridge University Press.

- Hahn, G. J., & Shapiro, S. S. (1967). *Statistical models in engineering*. (Tech. Rep.).
- Hernández-Lobato, J. M., & Adams, R. (2015). Probabilistic backpropagation for scalable learning of bayesian neural networks. In *International conference on machine learning* (pp. 1861–1869).
- Hoffman, M. D., Blei, D. M., Wang, C., & Paisley, J. (2013). Stochastic variational inference. *The Journal of Machine Learning Research*, *14*(1), 1303–1347.
- Hofmann, T., Schölkopf, B., & Smola, A. J. (2008). Kernel methods in machine learning. *The annals of statistics*, 1171–1220.
- Keeling, C., & Whorf, T. (1991). Mauna loa atmospheric co<sub>2</sub> modern record. *Trends*, *91*, 12–15.
- Kullback, S., & Leibler, R. A. (1951). On information and sufficiency. *The annals of mathematical statistics*, *22*(1), 79–86.
- Lakshminarayanan, B., Pritzel, A., & Blundell, C. (2017). Simple and scalable predictive uncertainty estimation using deep ensembles. In *Advances in neural information processing systems* (pp. 6402–6413).
- LeCun, Y., Bengio, Y., & Hinton, G. (2015). Deep learning. *nature*, *521*(7553), 436.
- LeCun, Y., Cortes, C., & Burges, C. J. (1998). The mnist database of handwritten digits, 1998. URL <http://yann.lecun.com/exdb/mnist>, *10*, 34.
- Liu, W., Principe, J. C., & Haykin, S. (2011). *Kernel adaptive filtering: a comprehensive introduction* (Vol. 57). John Wiley & Sons.

- MacKay, D. J. (1992). A practical bayesian framework for backpropagation networks. *Neural computation*, 4(3), 448–472.
- Meng, X., Zhang, J.-W., & Guo, H. (2016). Quantum brownian motion model for the stock market. *Physica A: Statistical Mechanics and its Applications*, 452, 281–288.
- Muandet, K., Fukumizu, K., Sriperumbudur, B., Schölkopf, B., et al. (2017). Kernel mean embedding of distributions: A review and beyond. *Foundations and Trends® in Machine Learning*, 10(1-2), 1–141.
- Nagel, J. B. (2017). *Bayesian techniques for inverse uncertainty quantification* (Unpublished doctoral dissertation). ETH Zurich.
- Neal, R. M. (2012). *Bayesian learning for neural networks* (Vol. 118). Springer Science & Business Media.
- Nguyen, A., Yosinski, J., & Clune, J. (2015). Deep neural networks are easily fooled: High confidence predictions for unrecognizable images. In *Proceedings of the ieee conference on computer vision and pattern recognition* (pp. 427–436).
- Osband, I., Blundell, C., Pritzel, A., & Van Roy, B. (2016a). Deep exploration via bootstrapped dqn. In *Advances in neural information processing systems* (pp. 4026–4034).
- Osband, I., Blundell, C., Pritzel, A., & Van Roy, B. (2016b). Deep exploration via bootstrapped dqn. In *Advances in neural information processing systems* (pp. 4026–4034).

- Paisley, J., Blei, D., & Jordan, M. (2012). Variational bayesian inference with stochastic search. *arXiv preprint arXiv:1206.6430*.
- Parzen, E. (1962). On estimation of a probability density function and mode. *The annals of mathematical statistics*, 33(3), 1065–1076.
- Parzen, E. (1970). *Statistical inference on time series by rkhs methods*. (Tech. Rep.). STANFORD UNIV CALIF DEPT OF STATISTICS.
- Pearce, T., Zaki, M., Brintrup, A., & Neel, A. (2018). Uncertainty in neural networks: Bayesian ensembling. *arXiv preprint arXiv:1810.05546*.
- Pradier, M. F., Pan, W., Yao, J., Ghosh, S., & Doshi-Velez, F. (2018). Latent projection bnns: Avoiding weight-space pathologies by learning latent representations of neural network weights. *arXiv preprint arXiv:1811.07006*.
- Principe, J. C. (2010). *Information theoretic learning: Renyi's entropy and kernel perspectives*. Springer Science & Business Media.
- Principe, J. C., Xu, D., Fisher, J., & Haykin, S. (2000). Information theoretic learning. *Unsupervised adaptive filtering, 1*, 265–319.
- Rasmussen, C. E. (2003). Gaussian processes in machine learning. In *Summer school on machine learning* (pp. 63–71).
- Rényi, A., et al. (1961). On measures of entropy and information. In *Proceedings of the fourth berkeley symposium on mathematical statistics and probability, volume 1: Contributions to the theory of statistics*.

- Shannon, C. E., & Weaver, W. (1949). *The mathematical theory of communication (urbana, il. University of illinois Press IL.*
- Silverman, B. W. (2018). *Density estimation for statistics and data analysis.* Routledge.
- Smith, R. C. (2013). *Uncertainty quantification: theory, implementation, and applications* (Vol. 12). Siam.
- Smola, A. J., & Schölkopf, B. (1998). *Learning with kernels* (Vol. 4). Citeseer.
- Su, J., Vargas, D. V., & Sakurai, K. (2019). One pixel attack for fooling deep neural networks. *IEEE Transactions on Evolutionary Computation.*
- Sullivan, T. J. (2015). *Introduction to uncertainty quantification* (Vol. 63). Springer.
- Theil, H., & Meisner, J. F. (1980). Simultaneous equation estimation based on maximum entropy moments. *Economics Letters*, 5(4), 339–344.
- Tibshirani, R. (1996). A comparison of some error estimates for neural network models. *Neural Computation*, 8(1), 152–163.
- Vapnik, V. (2013). *The nature of statistical learning theory.* Springer science & business media.